



# Measurement of the $t\bar{t}$ Production Cross-Section in Dilepton Final States at DØ using $5.3 \text{ fb}^{-1}$ of Data

The DØ Collaboration  
(Dated: March 10, 2010)

We present a measurement of the production cross-section for top-antitop events decaying into electron-muon, dimuon or dielectron plus jets final states in proton-antiproton collisions at  $\sqrt{s} = 1.96 \text{ TeV}$  using  $4.3 \text{ fb}^{-1}$  of integrated luminosity collected with the DØ detector from June 2006 to June 2009. The measured cross-sections after taking into account the corresponding branching ratios and assuming a top quark mass of  $172.5 \text{ GeV}$  are:

$$ee : \quad \sigma_{t\bar{t}} = 9.0_{-1.4}^{+1.6} (\text{stat}) \pm 1.4 (\text{syst}) \pm 0.7 (\text{lumi}) \text{ pb}$$

$$e\mu : \quad \sigma_{t\bar{t}} = 9.1_{-0.7}^{+0.8} (\text{stat}) \pm 1.0 (\text{syst}) \pm 0.6 (\text{lumi}) \text{ pb}$$

$$\mu\mu : \quad \sigma_{t\bar{t}} = 7.2_{-1.4}^{+1.5} (\text{stat})_{-1.4}^{+1.3} (\text{syst}) \pm 0.7 (\text{lumi}) \text{ pb.}$$

These results are combined with the  $1 \text{ fb}^{-1}$  result previously published [3] leading to:

$$\ell\ell : \quad \sigma_{t\bar{t}} = 8.4 \pm 0.5 (\text{stat})_{-0.8}^{+0.9} (\text{syst})_{-0.6}^{+0.7} (\text{lumi}) \text{ pb.}$$

*Preliminary Results for Winter 2010*

## I. INTRODUCTION

The top quark is the heaviest known fermion, and could decay into exotic particles e.g. a charged Higgs boson [1]. The inclusive top quark pair ( $t\bar{t}$ ) production cross section ( $\sigma_{t\bar{t}}$ ) can be measured from individual  $t\bar{t}$  decay channels and their predicted standard model branching ratios. Exotic top quark decays would lead to different observed values of the inclusive  $t\bar{t}$  production cross section in the different channels. It is therefore important to precisely measure  $\sigma_{t\bar{t}}$  in all channels and compare the results to the standard model prediction. Within the standard model each top quark is expected to decay approximately 99.8% of the time to a  $W$  boson and a  $b$  quark [2]. Dilepton final states arise when both  $W$  bosons decay leptonically and also include two energetic jets resulting from the hadronization of the  $b$  quarks. The detector signature includes missing transverse energy ( $\cancel{E}_T$ ) from the high transverse momentum ( $p_T$ ) of the neutrinos from the decays of the  $W$  bosons. The standard model  $t\bar{t}$  branching fractions are 1.8%, 3.2% and 1.8% [2] for the  $e^+e^-$ ,  $e^\pm\mu^\mp$  and  $\mu^+\mu^-$  channels respectively, including the leptonic decays of  $\tau$  leptons. The  $t\bar{t}$  production cross section in  $p\bar{p}$  collisions has been measured in dilepton final states using the datasets provided by Run II of the Tevatron [3, 4]. The updated  $D\bar{O}$  measurements presented here are based on data taken in the period between June 2006 and June 2009 which is called Run IIb and which corresponds, after data quality selection, to a measured integrated luminosity [5] of  $4.3 \text{ fb}^{-1}$ . We combine this updated measurement with the  $D\bar{O}$  dilepton published result from the first  $1 \text{ fb}^{-1}$  of Run II data [3].

## II. LEPTON AND JET IDENTIFICATION

The  $D\bar{O}$  detector has a central tracking system, consisting of a silicon microstrip tracker and a central fiber tracker, both located within a 2 T superconducting solenoidal magnet [6], designed for tracking and vertexing at pseudorapidities  $|\eta| < 3$  and  $|\eta| < 2.5$ , respectively. A liquid-argon and uranium calorimeter has a central section (CC) covering pseudorapidities  $|\eta|$  up to  $\approx 1.1$ , and two end calorimeters (EC) that extend coverage to  $|\eta| \approx 4.2$ , with all three housed in separate cryostats [7]. An outer muon system, at  $|\eta| < 2$ , consists of a layer of tracking detectors and scintillation trigger counters in front of 1.8 T toroids, followed by two similar layers after the toroids [8]. Luminosity is measured using plastic scintillator arrays placed in front of the EC cryostats. The trigger and data acquisition systems are designed to accommodate the high luminosities of Run II.

Electrons are identified as clusters of energy in calorimeter cells in a cone of size  $\Delta R = \sqrt{\Delta\phi^2 + \Delta\eta^2} = 0.4$ . Electron candidates are required to have a large fraction of their energy deposited in the electromagnetic layers of the calorimeter. The clusters are required to be isolated from hadronic energy deposition, to be matched to a charged track in the central tracking system and to have a shower shape consistent with that of an electron. We use both central ( $|\eta| < 1.1$ ) and forward ( $1.5 < |\eta| < 2.5$ ) electron candidates. In addition, we require the electrons to be selected by a likelihood discriminant that combines information both from the central tracking system and from the calorimeter in order to select prompt electrons.

Muon reconstruction begins with matching track segments between the inner muon layer and the two outer layers. A track in the central tracking system must also match the muon identified in the muon system, and the chi-squared of the overall track fit must be smaller than 4. To reject cosmic muons we apply requirements on the time of arrival of the muon at the different layers of scintillators in the muon system. All muons must be within  $|\eta| < 2.0$ . Muons originating from  $W$  (or  $Z$ ) decays are identified using two isolation criteria: (i) the energy deposited in the calorimeter in a hollow cone around the muon track direction is smaller than 15% of the energy of the muon itself (this fraction is referred to as "calorimeter isolation"), and (ii) the scalar sum of the transverse momenta of the charged tracks surrounding the muon track in the central tracking system is smaller than 15% of the muon track  $p_T$  (this fraction is referred to as "tracker isolation"). To enrich the proportion of muons originating from  $W$  decay we also require that the distance of closest approach of the muon track to the primary vertex is smaller than 0.04 cm for a muon track with a hit in the silicon microstrip tracker and smaller than 0.2 cm for a muon track without hits in the silicon microstrip tracker.

Jets are reconstructed with a fixed cone of radius,  $\Delta R = 0.5$  [9] and must be recognized as such by the independent calorimeter trigger readout. Jet energy scale corrections are applied to the jets [10]. The vectorial missing transverse momentum is reconstructed from the opposite of the vector sum of the transverse energies in all calorimeter cells for which the energy is significantly above the noise. It is further corrected by the transverse momentum of all reconstructed muons, as well as by the energy calibration corrections applied to the transverse momenta of electrons and jets.  $\cancel{E}_T$  is defined as the magnitude of the vectorial missing transverse momentum. A more detailed description of object reconstruction can be found in Ref. [11].

### III. EVENT SELECTION AND SIGNAL EFFICIENCY

We first select events with two isolated charged leptons  $\ell$  (either electron or muon) with  $p_T^\ell > 15$  GeV. The two leptons are required to be of opposite charge. Events are also required to contain at least two jets. Each of the jets must have transverse momentum  $p_T^j > 20$  GeV and  $|\eta| < 2.5$ . These events are also required to pass a trigger requiring one proto-electron candidate for the  $e^+e^-$  channel and one proto-muon candidate for the  $\mu^+\mu^-$  channel. Events used for the  $e^\pm\mu^\mp$  channel cross section measurement are selected with a mixture of electron and muon triggers, yielding a trigger efficiency close to 100%.

To reduce the background from  $Z/\gamma^*$ , diboson production and fake identified leptons we apply different final topological selections depending on the channel. The final selection in the  $e^\pm\mu^\mp$  channel requires  $H_T = p_T^{\ell 1} + \sum(p_T^j) > 110$  GeV, where  $p_T^{\ell 1}$  denotes the  $p_T$  of the leading lepton. In the  $e^+e^-$  and  $\mu^+\mu^-$  channels, boosted decision trees (BDT) [12] are used to discriminate between signal and background. The input variables used for the BDT are (see Ref. [13] for definitions): aplanarity, centrality, sphericity,  $H_T$ , the sum of the jets and lepton energies:  $H$ ,  $\cancel{E}_T$ , scaled  $\cancel{E}_T$  [14], the minimum distance in the  $\eta - \phi$  space between the closest pair of jets multiplied by the  $E_T$  of the lowest  $E_T$  jet in the pair, and divided by the  $E_T$  of the  $W$  ( $k'_{t\ min}$ ), the minimum dijet mass of all jet pairs ( $M_{jj\ min}$ ), and the dilepton invariant mass ( $M_{\ell\ell}$ ). The BDT have been trained on  $t\bar{t}$  Monte Carlo (MC) samples against  $Z/\gamma^* \rightarrow ee$  or  $\mu\mu$  and diboson MC samples. Maximizing  $S/\sqrt{S+B}$  where  $S$  is the number of signal events and  $B$  the number of background events, we find the optimal cuts on  $H_T$  or on the BDT discriminant outputs.

In order to compute the acceptances and efficiencies for the signal and to train the BDT, we generate  $t\bar{t}$  events at  $\sqrt{s} = 1.96$  TeV using the ALPGEN [15] matrix element generator assuming a top quark mass  $m_{top}$  of 172.5 GeV. These events are processed through PYTHIA [16] to simulate fragmentation, hadronization and decays of short-lived particles. The two  $W$ 's are forced to decay to lepton-neutrino pairs, including all  $\tau$  final states. These events are processed through a full detector simulation using GEANT [17], which provides tracking hits, calorimeter cell energy and muon hit information. We estimate the impact of detector noise and additional  $p\bar{p}$  interactions by adding hits from collider events gathered without a trigger bias to the MC events. The same reconstruction process is then applied to both data and simulated events.

### IV. BACKGROUND ESTIMATION

Several background processes can fulfill the selection criteria designed to select  $t\bar{t}$  events. We distinguish two categories of backgrounds: "physics" and "instrumental". Physics backgrounds are processes in which the charged leptons arise from electroweak boson decay. This signature comes from  $Z/\gamma^*$  events that decay leptonically (including leptonically decaying  $\tau$ 's) and from WW/WZ/ZZ (diboson) production. Instrumental backgrounds (or "fake" background) are defined as events in which a jet or a lepton within a jet is misidentified as an isolated lepton.

The selection efficiencies for the physics backgrounds  $Z/\gamma^* \rightarrow e^+e^-$ ,  $\mu^+\mu^-$  or  $\tau^+\tau^- \rightarrow \ell\ell'$  with  $\ell, \ell' = e$  or  $\mu$  are estimated using MC samples generated by ALPGEN and processed by PYTHIA while for WW/WZ/ZZ they are simulated using PYTHIA. The  $Z/\gamma^* \rightarrow \ell\ell$  and diboson processes are generated at leading order (LO) and are normalized to the next-to-next-to-leading order (NNLO) inclusive cross section for  $Z/\gamma^*$  and to the next-to-leading order (NLO) inclusive cross section for diboson [18]. As the  $Z$  boson  $p_T$  is not properly described in the ALPGEN simulation, we reweight the  $Z$  boson  $p_T$  distribution for different jet multiplicity bins using  $Z \rightarrow e^+e^-$  data events.

Fake electrons can arise from instrumental effects. Jets comprised essentially of a leading  $\pi^0/\eta$  and an overlapping or conversion-produced track, for example, can mimic an isolated high- $p_T$  electron. In the  $e^+e^-$  and  $e^\pm\mu^\mp$  analyses the amount of fake electron background is fitted to the observed distribution of electron likelihood in the data separately for CC and EC electrons prior to any likelihood cut. To this end we first determine the shape of the electron likelihood for real electrons in a pure  $Z/\gamma^* \rightarrow e^+e^-$  sample selected with the same requirements as in the dielectron channel but dropping the likelihood cut on one randomly chosen electron. The shape of the electron likelihood for the fake electron background is determined using a sample dominated by fake electrons by selecting one anti-isolated muon (both calorimeter and tracker isolation greater than 15%) with  $\cancel{E}_T < 15$  GeV. The number of fake electrons in the selected sample is obtained by performing an extended unbinned likelihood fit to the observed distribution of the electron likelihood in data.

A muon in a jet may appear isolated when the jet is not reconstructed. We measure the fraction of muons ( $f_\mu$ ) that appear as isolated in a dimuon control sample dominated by fake isolated muons. To suppress physics processes with real isolated muons in this sample the leading  $p_T$  muon is required to fail the muon isolation criteria. The other muon is then asked to be loosely isolated (both calorimeter and tracker isolation lower than 50%). In the  $e^\pm\mu^\mp$  channel, the contribution from events in which both leptons are fake leptons is already accounted for when computing the fake electron background and so it is subtracted before computation of the fake isolated muon background. The number

of fake isolated muons in the final  $e^\pm\mu^\mp$  and  $\mu^+\mu^-$  samples is computed from the number of events in a sample in which the two leptons have the same sign with loosely isolated muons times the previously measured fraction  $f_\mu$ .

## V. RESULTS

In Table I we summarize the predicted and observed number of events. The prediction for  $Z/\gamma^*$  background, misidentified leptons, and diboson backgrounds are also provided. Predicted and observed distributions for various event variables are shown in Fig 1.

TABLE I: The measured and predicted event yield for the different  $t\bar{t} \rightarrow \ell\ell$  processes. The errors are computed by adding statistical and systematic uncertainties (except the luminosity uncertainty) in quadrature.

	ee	$e\mu$	$\mu\mu$
$Z \rightarrow \ell\ell$	$8.5^{+3.4}_{-3.4}$	$11.9^{+2.7}_{-2.5}$	$21.7^{+5.6}_{-6.2}$
Dibosons	$2.1^{+0.8}_{-0.8}$	$6.5^{+2.1}_{-2.0}$	$3.3^{+1.1}_{-1.2}$
Instrumental background	$0.1^{+0.2}_{-0.1}$	$10.7^{+4.1}_{-3.9}$	$3.2^{+0.8}_{-0.7}$
$t\bar{t} \rightarrow \ell\ell jj$ ( $\sigma = 7.45$ pb)	$36.9^{+3.8}_{-3.8}$	$143.4 \pm 14.3$	$45.1^{+4.4}_{-4.3}$
Total expected events	$47.6 \pm 6.2$	$172.6^{+16.5}_{-16.4}$	$73.3^{+8.1}_{-8.8}$
Data	55	204	72

The  $t\bar{t}$  cross section in the individual dilepton channels is extracted by minimizing a negative log-likelihood function based on the Poisson probability of observing a number of events, given the luminosity, branching fraction,  $t\bar{t}$  efficiency and a number of background events. The combined cross section is measured by minimizing the sum of the negative log-likelihood functions for each individual channel [19].

The systematic uncertainty on the dilepton cross section measurement is obtained by varying the efficiencies and background contributions within their errors, taking all the correlations between the channels and between the different classes of background into account. The dominant systematic uncertainties are summarized in Table II.

TABLE II: Summary of the systematic uncertainties on the  $t\bar{t} \rightarrow \ell\ell$  cross section measurements in percent of the cross sections in each channel and for the combinations.

	ee, %	$e\mu$ , %	$\mu\mu$ , %	$\ell\ell$ , % (Run IIb)	$\ell\ell$ , % (Run II)
Signal modeling	4.9	4.8	4.8	$+5.0$ $-4.7$	$+4.9$ $-4.6$
MC background normalisation	5.8	2.3	11.1	$+3.4$ $-3.3$	$+3.1$ $-3.0$
Instrumental background	0.4	2.3	1.7	1.6	$+1.4$ $-1.4$
Electron ID	8.9	3.9		$+4.2$ $-3.9$	$+3.3$ $-3.2$
Muon ID		1.7	4.9	$+1.9$ $-1.9$	$+1.6$ $-1.5$
Jet ID and resolution	6.5	3.2	$+5.9$ $-9.3$	$+4.2$ $-3.9$	$+3.4$ $-3.2$
Jet energy scale	6.9	4.9	7.6	$+5.6$ $-5.2$	$+5.2$ $-4.9$
Trigger	0.6	5.5	7.9	$+4.1$ $-3.7$	$+3.2$ $-3.1$
Others	3.8	2.5	3.4	$+2.8$ $-2.7$	$+2.7$ $-2.6$
<b>Total:</b>	$\pm 15.5$	$\pm 11.1$	$+18.4$ $-19.8$	$+11.5$ $-10.9$	$+10.3$ $-9.8$

The following main systematics have been studied:

- **Signal modeling:** The variation of  $t\bar{t}$  efficiency due to hadronization modeling, color reconnection or higher order effects using different MC generators and tunes is quoted as systematic uncertainty. We also include uncertainties coming from parton distribution functions, variation of the amount of initial and final state radiations and from different b-fragmentation modeling.
- **MC background statistics and normalization:** Half of the ratio of the NLO cross section divided by the LO cross section which was used to scale the PYTHIA diboson MC cross sections is taken as the systematic

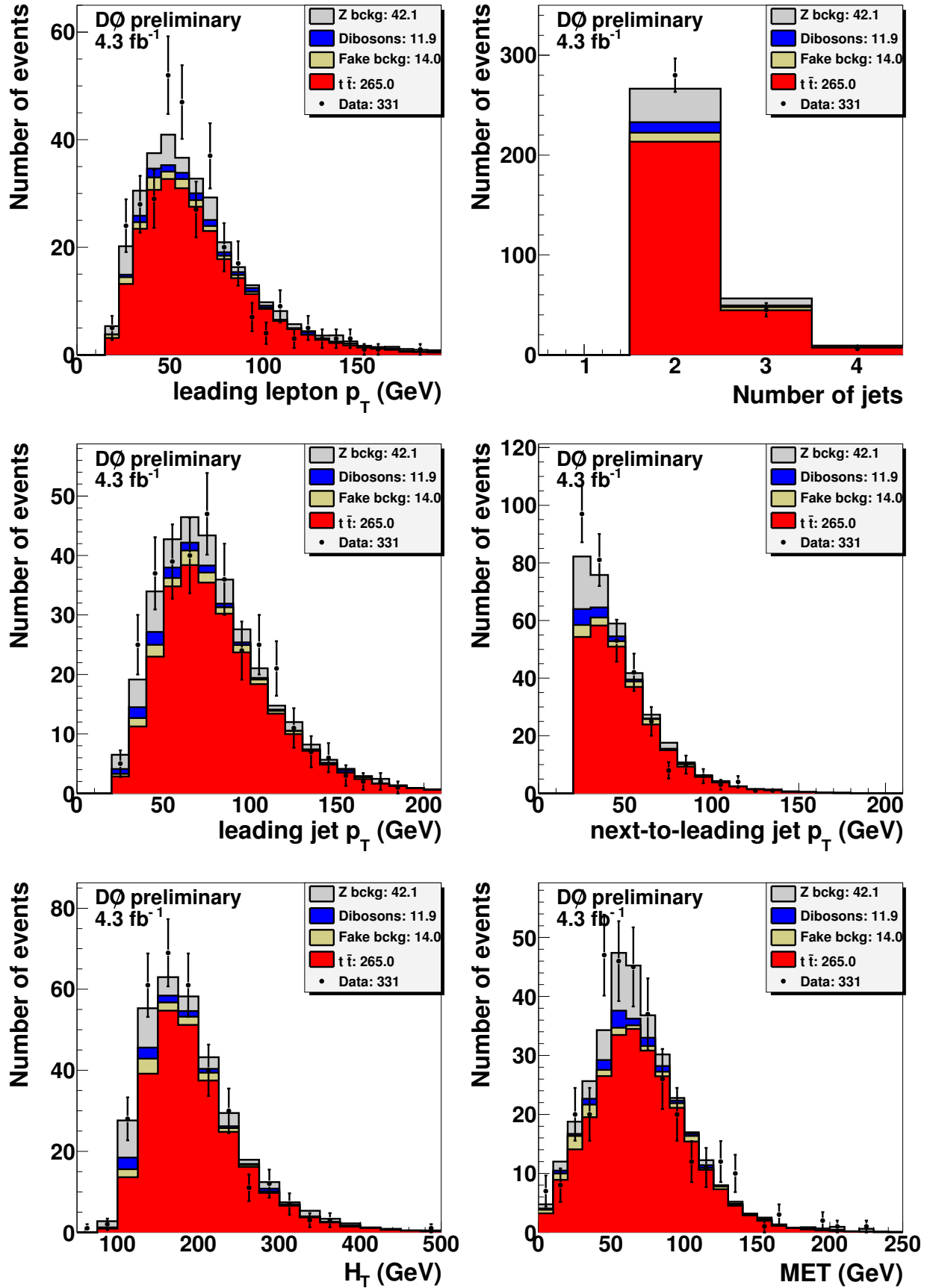


FIG. 1: Observed and predicted distributions for various backgrounds and the signal after the final selection requirements for the three dilepton channels. The  $t\bar{t}$  signal is normalized to the combined measured cross section (eq. 1).

uncertainty for the diboson background. Varying the  $Z$  boson  $p_T$  reweighting function contributes to the systematic uncertainty on the  $Z/\gamma^*$  background normalization. Another contribution comes from the uncertainty on the NNLO  $Z/\gamma^*$  theoretical cross section. We also include here the uncertainty that originates from the statistical error on the selection efficiencies and on the  $W \rightarrow \ell\nu$  branching ratio [2].

- **Instrumental background:** The shape of the electron likelihood discriminant is used to fit the number of fake electrons in the final selected sample. The shape itself is found to be dependent on the electron  $p_T$ . The number of fake electrons is fitted with the various shapes to extract the systematic uncertainty on this background. The statistical error on the fit is also propagated to the estimated number of fake electron background. The statistical error on the muon isolation fake rate  $f_\mu$  and on the size of the same sign lepton samples used to estimate the number of fake muon background are also included in this uncertainty.
- **Electron and muon identification:** The lepton identification efficiencies are measured in the data using well understood processes like  $Z/\gamma^* \rightarrow ee$  or  $Z/\gamma^* \rightarrow \mu\mu$  using the tag and probe method. They are studied and parametrized in various detector regions and various jet environments. Residual dependencies of the ratio of data to MC efficiencies are treated as systematic uncertainties. These uncertainties also include uncertainties related to energy scale difference between data and MC.
- **Jet identification and resolution:** Jet reconstruction efficiency and jet resolution are determined in data and the corresponding corrections are applied to MC. Uncertainties related to the methods and to the data to MC corrections are propagated to signal and background predictions.
- **Jet energy scale:** The measured jet energies in the calorimeter are corrected for the response of the calorimeter, for jet showering outside the jet reconstruction cone and for energy from underlying activity in the event [10]. The uncertainty on the jet energy calibration is propagated to the predicted background yields and to the efficiency for the  $t\bar{t}$  signal. The uncertainty due to the different response between jets from light quarks, jets from  $b$  quarks and jets from gluons is also taken into account.
- **Trigger efficiency:** Trigger efficiencies are derived from data. We assign as systematic error the variation of the data and MC difference when applying explicit trigger requirements on only one of the lepton.
- **Others:** These include the uncertainties on the efficiency of removing noisy events, on the lepton opposite sign requirement and the difference observed in vertex distributions and vertex selection criteria between data and MC.

Our preliminary measurements of the  $t\bar{t}$  production cross sections at  $\sqrt{s} = 1.96$  TeV in the dilepton channel assuming a top quark mass of 172.5 GeV using  $4.3 \text{ fb}^{-1}$  of integrated luminosity are:

$$\begin{aligned}
 ee : \quad \sigma_{t\bar{t}} &= 9.0_{-1.4}^{+1.6} \text{ (stat)} \pm 1.4 \text{ (syst)} \pm 0.7 \text{ (lumi) pb;} \\
 e\mu : \quad \sigma_{t\bar{t}} &= 9.1_{-0.7}^{+0.8} \text{ (stat)} \pm 1.0 \text{ (syst)} \pm 0.6 \text{ (lumi) pb;} \\
 \mu\mu : \quad \sigma_{t\bar{t}} &= 7.2_{-1.4}^{+1.5} \text{ (stat)}_{-1.4}^{+1.3} \text{ (syst)} \pm 0.7 \text{ (lumi) pb.}
 \end{aligned}$$

Combining the cross sections for the three channels above leads to:

$$\ell\ell_{\text{Run IIb}} : \quad \sigma_{t\bar{t}} = 8.8 \pm 0.6 \text{ (stat)} \pm 1.0 \text{ (syst)}_{-0.6}^{+0.7} \text{ (lumi) pb.} \tag{1}$$

This result is in agreement with the previous result of  $7.5_{-1.3}^{+1.6}$  pb [3]. Then we combine this result with the  $D\bar{O} \ell\ell$  published result [3] that used  $1 \text{ fb}^{-1}$  of integrated luminosity taking the proper correlations into account. This leads to a  $t\bar{t}$  production cross section in the dilepton channel for a top quark mass of 172.5 GeV using  $5.3 \text{ fb}^{-1}$  of integrated luminosity of:

$$\ell\ell : \quad \sigma_{t\bar{t}} = 8.4 \pm 0.5 \text{ (stat)}_{-0.8}^{+0.9} \text{ (syst)}_{-0.6}^{+0.7} \text{ (lumi) pb.}$$

The measured cross sections are in agreement with the standard model prediction of  $7.46_{-0.67}^{+0.48}$  pb [20], as can also be seen in Fig. 2 which shows the variation of the measured combined cross section as a function of top quark mass, compared to different theoretical calculations.

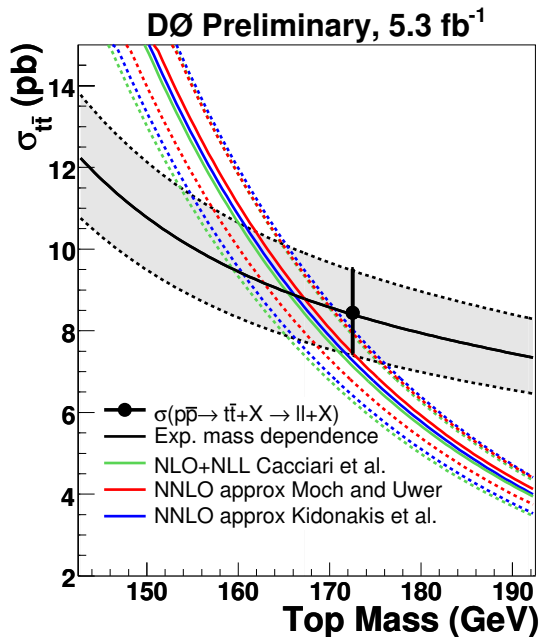


FIG. 2: Variation of the combined  $t\bar{t}$  production cross section as measured in the dilepton channels (point) as a function of the top quark mass fitted using the same function as in [3]. The black line is computed by measuring the variation of the  $t\bar{t}$  efficiency as a function of the top quark mass. The red, green and blue line shows the theoretical predictions from [20–22].

## VI. ACKNOWLEDGEMENTS

We thank the staffs at Fermilab and collaborating institutions, and acknowledge support from the DOE and NSF (USA); CEA and CNRS/IN2P3 (France); FASI, Rosatom and RFBR (Russia); CNPq, FAPERJ, FAPESP and FUNDUNESP (Brazil); DAE and DST (India); Colciencias (Colombia); CONACyT (Mexico); KRF and KOSEF (Korea); CONICET and UBACyT (Argentina); FOM (The Netherlands); STFC and the Royal Society (United Kingdom); MSMT and GACR (Czech Republic); CRC Program and NSERC (Canada); BMBF and DFG (Germany); SFI (Ireland); The Swedish Research Council (Sweden); and CAS and CNSF (China).

- 
- [1] J.F. Gunion *et al.*, *The Higgs Hunters Guide*, Addison-Wesley, Redwood City, California, 1990, p.200.
  - [2] C. Amsler *et al.* [Particle Data Group], *Phys. Lett. B* **667**, 1 (2008).
  - [3] V. M. Abazov *et al.* [D0 Collaboration], *Measurement of the  $t\bar{t}$  production cross section and top quark mass extraction using dilepton events in  $p\bar{p}$  collisions*, *Phys. Lett. B* **679**, 177 (2009).
  - [4] A. Abulencia *et al.* [CDF Collaboration], *Cross section measurements of high- $p(T)$  dilepton final-state processes using a global fitting method*, *Phys. Rev. D* **78**, 012003 (2008).
  - [5] T. Andeen *et al.* [D0 Collaboration], FERMILAB-TM-2365 (2007).
  - [6] V. M. Abazov *et al.* [D0 Collaboration], *The Upgraded D0 Detector*, *Nucl. Instrum. Meth. A* **565** (2006) 463.
  - [7] S. Abachi *et al.* [D0 Collaboration], *The D0 Detector*, *Nucl. Instrum. Meth. A* **338**, 185 (1994).
  - [8] V. M. Abazov *et al.*, *The muon system of the Run II D0 detector*, *Nucl. Instrum. Meth. A* **552**, 372 (2005).
  - [9] G. C. Blazey *et al.*, [arXiv:hep-ex/0005012].
  - [10] B. Abbott *et al.* [D0 Collaboration], *Nucl. Instrum. Meth. A* **424**, 352 (1999).
  - [11] V. M. Abazov *et al.* [D0 Collaboration], *Phys. Rev. D* **76**, 052006 (2007).
  - [12] L. Breiman *et al.*, *Classification and Regression Trees* (Wadsworth, Stamford, 1984);  
J.A. Benitez, Ph.D. thesis, Michigan State University, 2009;  
D. Gillberg, Ph.D. thesis, Simon Fraser University, 2009.
  - [13] V. D. Barger, J. Ohnemus and R. J. N. Phillips, *Phys. Rev. D* **48** (1993) 3953.
  - [14] V. M. Abazov *et al.* [D0 Collaboration], *Phys. Rev. Lett.* **96** (2006) 011801.
  - [15] M.L. Mangano, M. Moretti, F. Piccinini, R. Pittau, A. Polosa, *ALPGEN, a generator for hard multiparton processes in hadronic collisions*, *JHEP* **0307** (2003) 1.

- [16] T. Sjöstrand, L. Lönnblad, S. Mrenna and P. Skands, [arXiv:hep-ph/0308153];  
T. Sjöstrand, P. Edén, C. Friberg, L. Lönnblad, G. Miu, S. Mrenna and E. Norrbin, *Comp. Phys. Commun.* **135** (2001) 238.
- [17] R. Brun and F. Carminati, CERN Program Library Long Writeup W5013, 1993 (unpublished).
- [18] J. M. Campbell and R. K. Ellis, *Phys. Rev. D* **60** (1999) 113006.
- [19] V. M. Abazov *et al.* [D0 Collaboration], *Phys. Rev. D* **80**, 071102 (2009).
- [20] S. Moch and P. Uwer, *Phys. Rev. D* **78** (2008) 034003.
- [21] M. Cacciari *et al.*, *JHEP* **09** (2008) 127.
- [22] N. Kidonakis, R. Vogt, *Phys. Rev. D* **78** (2008) 074005.